A MINI-RF RADAR ANALYSIS OF THE MOON'S SOUTH POLE-AITKEN BASIN. T. M. Aldridge[1], B. J. Thomson[2], P. R. Stoddard[1], J. T. S. Cahill[3], D. B. J. Bussey[3], and the Mini-RF Science Team, [1]Department of Geology and Environmental Science, Northern Illinois University, DeKalb, IL, [2]Boston University Center for Remote Sensing, Boston, MA, [3]The Johns Hopkins University Applied Physics Laboratory, Laurel, MD, (taldridge@niu.edu).

Introduction: Previous studies have shown a correlation between returned radar backscatter strength and lunar regolith composition [e.g., 1-3]. In particular, a comparison of Earth-based radar backscatter with multispectral Clementine-derived TiO_2 and FeO estimates of Mare Imbrium, Mare Fecunditatis, Mare Tranquilitatis, and Oceanus Procellarum suggest a correlation [4]. Earth-based 70-cm radar studies suggest a correlation between low CPR and high TiO_2 content and, conversely, between high CPR and low TiO_2 [5]. These studies are significant as it implies that radar can be used to estimate and potentially corroborate multispectral, gamma-ray, and neutron derived estimates of Fe-Ti oxide abundance. However, the use of radar as a compositional analysis tool requires better characterization and development.

Earth-based radar data sets are limited to perspectives of the lunar nearside. The South Pole-Aitken (SPA) basin, located on the southern farside, has been briefly characterized at radar wavelengths [6] and is an area of great scientific interest as it may have excavated lower-crust, perhaps even lunar mantle materials [7]. The Mini-RF instrument on NASA's Lunar Reconnaissance Orbiter (LRO) has allowed the collection of some of the first global radar coverage including significant coverage of SPA basin [8]. Here we use this data set to search for potential correlations between SPA radar backscatter and Clementine-derived TiO_2 estimates.

Regional Geology: The SPA basin is geologically diverse. The basin is pre-Nectarian in age and is the oldest and largest lunar basin on the Moon [9]. SPA is centered at 56ºS and 180ºW. It has a a diameter of 2500 km [10] and a rim to basin floor depth of 12 km [11]. The basin also exhibits rings at the outer 2500 km crest, a 2000 km depression, and a possible inner ring at 1800 km [12].

Instruments and Data Sets: The Miniature Radio Frequency (Mini-RF) is a synthetic aperture radar (SAR) aboard NASA's LRO mission. The instrument operates in S-band (12.6-cm) and X-band (4-cm). Clementine, launched in 1994, included UV-VIS-NIR instruments designed to map the global mineral signatures on the Moon [12].

Methods: Using Mini-RF S-band zoom (30m resolution) we derive the Stokes (S_1), the circular polarization ratio (CPR), and same sense (SC) parameters. The S_1 parameter represents the total average power of the returned radar signal. The circular polarization ratio (CPR) is the ratio of same sense and opposite sense (SC/OC) of the returned signal. SC polarization (depolarized echoes) result from double-bounces or diffuse scattering whereas OC polarization (polarized echoes) result from single-bounce or mirror-like scattering or quasi-specular reflection [3]. CPR is useful for roughness From global Clementine UVVIS-NIR data, we derive estimated TiO_2 maps using the methods of [13,14] for comparison with radar data products.

Three analyses were completed using each parameter. An initial study selected 19 cropped regions (Figure 1) within SPA craters that displayed varying concentrations of TiO_2. These regions ranged in size from 4×2 to 10×10 pixels. The next analysis used the initial crater regions and calculated the average and standard deviations of the geologic map polygons they were located in. These polygons allowed for a collection of a larger amount of pixels. The final analysis used geologic map polygons of selected rough regions in SPA to serve as a comparison to the smoother mare regions.

Results:

Analysis of Craters: Across the subareas selected within 19 study areas from craters across SPA, no correlation was found for S1 (Figure 2), CPR, or SC and TiO_2 weight percents. The data displays a range of TiO_2 (0.61 to 6.73 wt%). Each plot shows large error bars, each representing as much as 73.5% of the average value. This illustrates the large amount of roughness present for each subarea.

Geologic Map Analysis: In an attempt to reduce the size of the standard deviations across the study regions, an analysis was performed using the geologic map polygons that contain our 19 study areas. Similar to the subarea analysis, no correlation is evident (Figure 3). On average, the standard deviations are lower than those in the subarea analysis.

Geologic Map Analysis of Rough Regions: As a test of lunar roughness in SPA, an ArcMap analysis was performed using crater and terra regions. The resulting analysis shows a pattern similar to that of the subarea and geologic map analyses.

Discussion: Several factors may be affecting the lack of correlation found for Mini-RF radar and Clementine TiO_2 concentrations across SPA. CPR values for low to moderate TiO_2 concentrations for

mare basalts have been shown to be greater than that terrestrial lava flows [15]. Across SPA basin, concentrations for TiO_2 peak at under 7 wt% on average, thereby possibly contributing to a lack of correlation for the CPR parameter. Another factor is the use of the geologic map and the offset of polygons from the radar and Clementine data. The use of an updated geologic map could provide more accurate results. Many geologic contacts are not evident in Mini-RF radar (Figure 4), possibly due to the need for an updated geologic map. Mini-RF backscatter displays a large amount of variation in each polygon, possibly due to the crosstrack gradient. At the present time, only semi-emprical corrections are available for this.

Summary: We present a preliminary analysis of SPA basin using for Clementine-derived TiO_2 and Mini-RF derived S_1, CPR, and SC data products. The results indicate no correlation among the radar parameters and TiO_2 concentrations across the basin. With the implementation of an updated geologic map and solution for the crosstrack gradient, a future correlation may be found.

References: [1] Thompson T. W. (1970) *Radio Science, 5*, 253-262. [2] Pollack J. B. and Whitehill L. (1972) *JGR*, 77, 4289-4303. [3] Hagfors (1967) *Radio Science* 2, 5, 445-465. [4] Campbell B.A. et al. (1997) *JGR* 102, doi:10.1029/97JE00858. [5] Campbell B. A. et al. (2009) *GRL*, *36*, L22201, doi:10.1029/2009GL041087. [6] Aldridge T.A. et al. (2011) *LPSC 42* Abstract # 1883. [7] Pieters C. M. et al. (2001) *JGR*, *106*(E11), 28,001-28,022. [8] McAdams M. et al. (2010) *LPSC 42*. [9] Head J. W. et al. (1993) *JGR*, *98*(E9), 17,149-17,181. [10] Wilhelms D. (1987) *USGS Prof. Pap. 1348*, 302 pp. [11] Spudis P. D. et al. (1994) *Science*, *266*(5192), 1848-1851. [12] Nozette S. et al. (1994) *Science*, *266*(5192), 1835-1839. [13] Gillis J. J. et al. (2003) *JGR*, *108*, 5009, doi:10.1029/2001JE001515. [14] Gillis J. J. et al. (2004) *GCA*, 68, 3791-3805. [15] Campbell et al. (2010) Icarus, 208, 565-57.

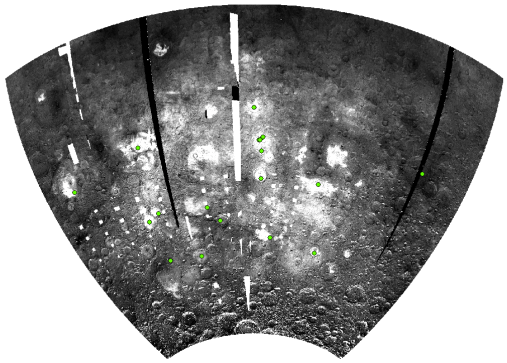

Figure 1. Location of the 19 study areas in SPA.

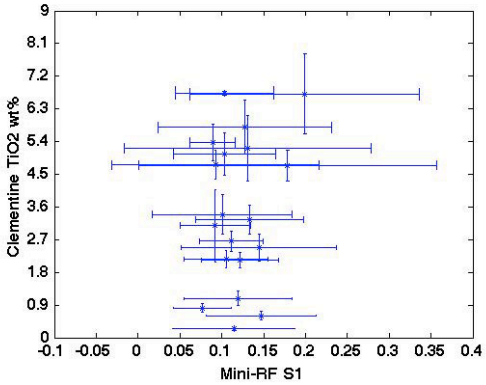

Figure 2. Analysis of craters using S1. The error bars are one standard deviation in length.

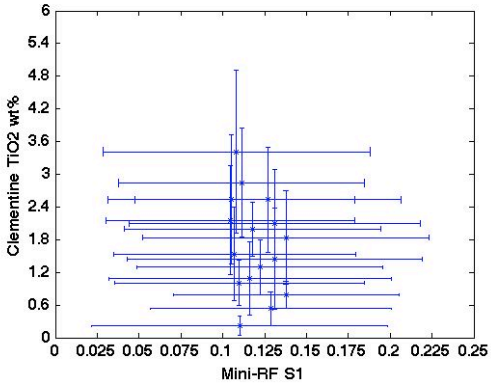

Figure 3. Geologic map analysis using S1. The error bars are one standard deviation in length.

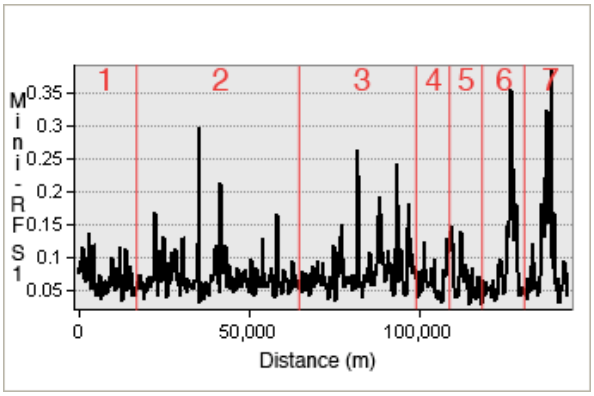

Figure 4. 3D analyst using orbit 4730, 35ºS 149ºE, Mini-RF S1. Regions: 1. Crater material, 2. Mare, 3. Fresh irregular terra, 4. Crater material, 5. Smooth light plains, 6. Crater material, 7. Grooves and mounds material.